Transition Metal Ion FRET in the Gas Phase: A 10-40 A Range Molecular Ruler for Mass-Selected Biomolecular Ions

Author(s):
Tiwari, Prince; Wu, Ri; Metternich, Jonas B.; Zenobi, Renato

Publication date:
2021-08-04

Permanent link:
https://doi.org/10.3929/ethz-b-000501422

Originally published in:
Journal of the American Chemical Society 143(30), https://doi.org/10.1021/jacs.1c01915

Funding acknowledgement:
ETH-07 15-1 - Native Biomolecular Ions in the Gas Physe? A Functional and Structural Approach (ETHZ)

Supporting Information

Transition metal ion FRET in the gas phase: a 10 - 40 Å range molecular ruler for mass-selected biomolecular ions

Prince Tiwari, Ri Wu, Jonas B. Metternich, and Renato Zenobi

Department of Chemistry and Applied Biosciences, ETH Zürich
Vladimir-Prelog-Weg 3, 8093 Zürich (Switzerland)
Email: zenobi@org.chem.ethz.ch

Contents

1. Dye labeled peptides

Peptide sequences were selected based on a previous publication on tmFRET in solution.[1] The rhodamine 110 dye-labeled peptides were commercially obtained (from Thermo Fisher Scientific, USA) in lyophilized form, with N-terminal acetylation and C-terminal amidation. The samples were dissolved at a concentration of 200 µM (stock solution) and diluted as required for the experiments.

Peptide sequences:

C2H3H7 : A[C]HAAKHAKAAAAAKA

C2H6H10 : A[C]AAKHAAKHAAAAKA

C2H10H14 : A[C]AAKAAAKHAAAHKA

Cysteine (marked [C]) was labeled with rhodamine 110 using a linker.

2. Mass-selected fluorescence measurements

The instrument and methodology to measure gas-phase fluorescence spectra are described elsewhere.[2] A 20 µM dye-labeled peptide sample was mixed with an equal volume of a 200 µM $CuCl_2$ solution and loaded into a pulled capillary for nanoESI. A potential (~1 kV) was applied to the solution using a platinum wire to obtain a steady electrospray. After traveling through the ion optics of the mass spectrometer, the ions were accumulated for 1 s and trapped in the ion trap (q_z = 0.8). The helium buffer gas pressure in the trap was kept high (2.1 mTorr) to increase the fluorescence signal relative to photodissociation. Mass selection was performed, i.e., all other ions were ejected. The mass-selected ions were irradiated for 1 s with a laser beam at a wavelength of 460 nm and suitable laser power (low mW range, typically between 1-6 mW) to obtain <5% photo-fragmentation. The emitted fluorescence was collected with a plano-convex lens placed in a hole drilled in the ring electrode of the ion trap. The large fluorescence collection solid angle of the lens allowed high fluorescence collection efficiency (~2%). The collected fluorescence was collimated and sent to a fluorescence detection system that could perform spectrally-resolved fluorescence measurements with a spectrograph and electrothermally-cooled CCD. The time-resolved fluorescence measurement was performed with a Single-Photon Avalanche Diode (SPAD) using Time-Correlated Single Photon Counting (TCSPC).

3. Fluorescence lifetimes

FRET efficiencies can be calculated by monitoring changes in either the donor's fluorescence spectrum or its fluorescence lifetime. However, to compare the fluorescence intensities, the mass spectral intensities should also be comparable. This might not always be the case as the mass detection efficiency depends on multiple factors that include mass, charge state, etc. Thus, fluorescence lifetimes were used to calculate FRET efficiencies as they yielded a single value, independent of the mass spectral intensity.

For fluorescence decay measurements to obtain fluorescence lifetimes, the repetition rate of the laser beam was reduced to 20 MHz. The lower repetition rate of the laser resulted in a sufficient time interval between two laser pulses for the excited dye to relax. The ions were accumulated in the ion trap for 1 s, mass-selected, and then irradiated with the laser beam for another 1 s. Fluorescence decay measurements were performed for 2000 s by repeating this sequence multiple times. The fluorescence signals from the trapped ions were low and often in the range of 10^3 counts/second. Compared with the repetition rate of the excitation laser (20 MHz), the chances of artifacts like pile up were thus low. The

same experiment was repeated without ions in the trap to obtain a background, which was later subtracted from the signal spectrum to obtain the fluorescence decay of the dye-labeled to the peptide. To ensure the stability of the signal, decays were recorded before and after the signal measurement and subtracted to check for any divergences. The fluorescence decays were fit with an exponentially modified Gaussian to extract the fluorescence lifetimes as the decay is a convolution of the instrument response function (approximated as a Gaussian) and an exponential fluorescence decay. The width of the fitted Gaussian was always found to be around 100s of ps, similar to the width of the experimentally obtained instrument response function. Single exponential fits were found to be enough to yield the lifetimes (Figure 4 & 5), and no oscillations in the residuals were noticed. Experiments were repeated over multiple days and the reported lifetimes are an average of different measurements. The reported errors are the propagated errors obtained from the respective fit of the fluorescence decays. A double exponential fit to the decays also gave only one dominant component (>90%), whose values were comparable with those obtained from single-exponential fits (Table S1).

Table S1: Fluorescence lifetimes and tmFRET efficiencies obtained from fitting the fluorescence decays with a Gaussian modified double exponential function.

Species	Relative amplitude	Lifetime (ns)	χ^2	tmFRET Efficiency
$(C3H4H7)^{3+}$	$A_1 = 0.05$ $A_2 = 0.95$	$\tau_1 = 25.0$ $\tau_2 = 5.91$	5.2	-
$(C2H3H7+Cu)^{5+}$	$A_1 = 0.11$ $A_2 = 0.89$	$\tau_1 = 17.9$ $\tau_2 = 1.49$	9.9	0.75
$(C2H6H10)^{3+}$	$A_1 = 0.04$ $A_2 = 0.96$	$\tau_1 = 25.0$ $\tau_2 = 6.04$	2.5	-
$(C2H6H10+Cu)^{5+}$	$A_1 = 0.10$ $A_2 = 0.90$	$\tau_1 = 24.6$ $\tau_2 = 3.45$	3.9	0.43
$(C2H10H14)^{3+}$	$A_1 = 0.04$ $A_2 = 0.96$	$\tau_1 = 25.0$ $\tau_2 = 5.95$	4.2	-
$(C2H10H14+Cu)^{5+}$	$A_1 = 0.94$ $A_2 = 0.06$	$\tau_1 = 25$ $\tau_2 = 3.95$	7.2	0.34

4. Control experiments

Different control measurements were performed to rule out any other phenomenon and establish the occurrence of tmFRET. Key control experiments and their results are described below:

a) High-affinity binding of Cu^{2+} to di-his-containing peptides: The high-affinity binding of Cu^{2+} to the histidine pair in the peptides has been demonstrated in the literature for solution-phase experiments.[1] To confirm the binding of Cu^{2+} ions to gaseous peptide ions, two peptide sequences, one without and the other with histidine pairs, were electrosprayed from solutions with tenfold excess Cu^{2+} ions. It can be seen from the mass spectra that the peptide sequence without the histidine pair barely showed any Cu^{2+} adducts (Figure S1a), whereas the peptide sequence with Cu^{2+} had multiple Cu^{2+} adduct peaks in the mass spectrum (Figure S1b). In a similar peptide sequence with single histidine, the binding was also not found to be very effective. This observation confirmed that the binding of Cu^{2+} ions with peptides containing histidine pairs was selective in nature.

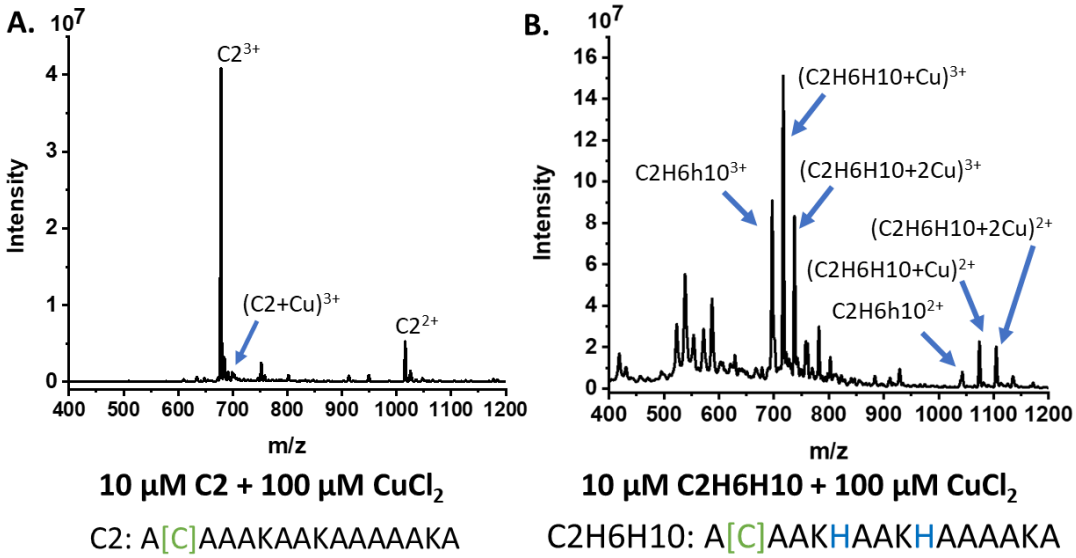

Figure S1: A) Peptide sequence without his; B) peptide sequence with di-his. Higher binding in the presence of histidine pair can be observed.

b) **Fluorescence spectrum and laser power dependence**: Similar fluorescence spectra from dye-labeled peptides, without and with bound Cu^{2+} were observed, showing that the photophysics of the dye was not altered upon binding with Cu^{2+} ions (Figure S2). The fluorescence lifetime of the dye-labeled peptides and their complexes with Cu^{2+} were also not found to change in the range of power that was measured (3 – 10 mW), showing that the peptide structure did not change drastically upon laser excitation.

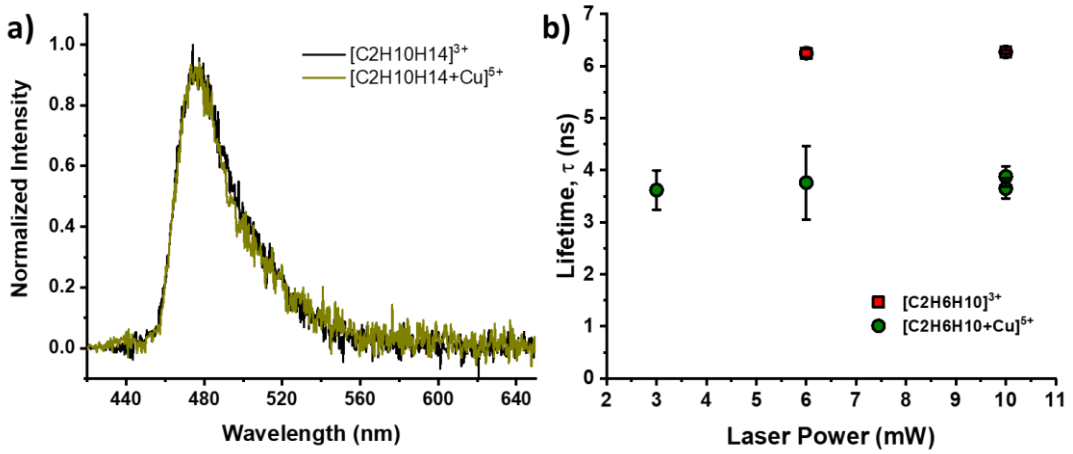

Figure S2: a) Fluorescence spectra of the dye-labeled peptide C2H10H15 in the 3+ charge state and it's complex with Cu^{2+} in 5+ charge states. b) Fluorescence lifetime of $[C2H6H10]^{3+}$ and $[C2H6H10+Cu]^{5+}$ at different laser powers. No significant change in the fluorescence lifetime indicated that the laser excitations did not cause a significant change in peptide structure. Error bars represent corresponding error in the fit. (Fluorescence lifetime of $[C2H6H10+Cu]^{5+}$ was not acquired.)

c) Higher charge and non-tmFRET metal ions do not lead to a decrease in fluorescence lifetime: The change in the fluorescence lifetime of the dye-labeled to the peptide in the 5+ charge state and upon binding with a non-transition metal FRET ion, Zn^{2+}, was minimal compared to the change upon binding with a transition metal FRET ion (Figure S3), Cu^{2+}. The higher error in the case of Zn^{2+} complexed peptide originated from its low mass spec signal intensity, resulting in poor signal-to-noise in the fluorescence decay.

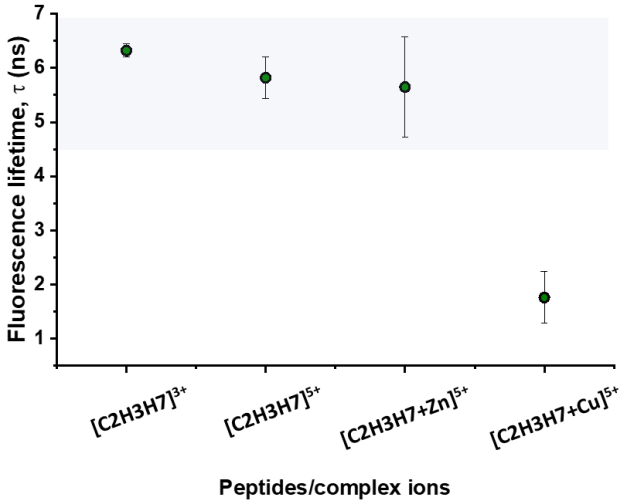

Figure S3: Fluorescence lifetime of C2H3H7 in different charge states and complexation. Shortening in fluorescence lifetime was observed only when complexing with copper.

d) Ni^{2+} also leads to a decrease in fluorescence lifetime: tmFRET was also observed with another tmFRET ion, Ni^{2+}. The decrease in fluorescence lifetime with Ni^{2+} (Figure S4) was higher as the spectral overlap of the donor emission is higher with the Ni^{2+} absorption.

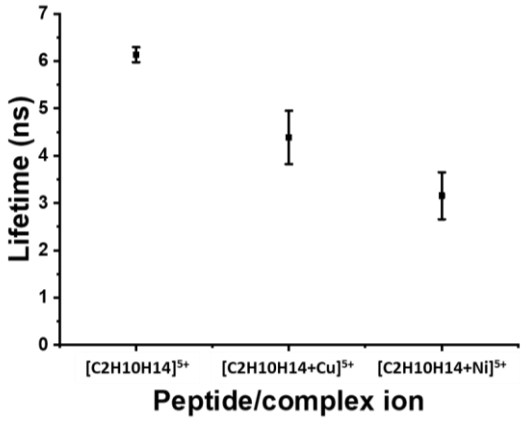

Figure S4: Decrease in fluorescence lifetime of R110 when tmFRET ions, Cu^{2+} and Ni^{2+}, binds with the peptide.

e) **Decrease in fluorescence lifetime observed with another fluorescent dye as donor:** for a control measurement using another donor dye, the peptide (Sequence: Ac-CAARAHAAAHARAARA-NH2) was obtained from Genscript Biotech (Piscataway, NJ, USA) at a purity of 92%. The thiol functional group of cysteine was found to be non-oxidized, so the labeling procedure was performed without further reduction or purification. Carboxy-rhodamine 6G maleimide (mixture of 5 and 6 isomer) was obtained from Setareh Biotech and used without further purification. A phosphate buffer (100 mM), containing guanidium chloride (6M) for increased solubility, was prepared and the pH adjusted to 7.1. C2H6H10 (1.5 mg) was dissolved in the phosphate-buffer solution (300 uL) and the dye (0.2 mg) was added in a solution of dimethylformamide (20 uL). The reaction mixture was stirred vigorously and stored on ice for 2 hours. The reaction was quenched by addition of 1 M dithiothreitol solution (10 uL) and purified by reversed phase HPLC (C18 column: Reprosil Gold 200; Dr. Maisch GmbH, Ammerbach, Germany). Mass spectrum of the purified sample was measured (Figure S5a) and confirmed the labeling. The gas-phase fluorescence spectrum of 3+ charge state of the labeled peptide also showed overlap of the donor emission and acceptor absorption, indicating the possibility of tmFRET (Figure S5b).

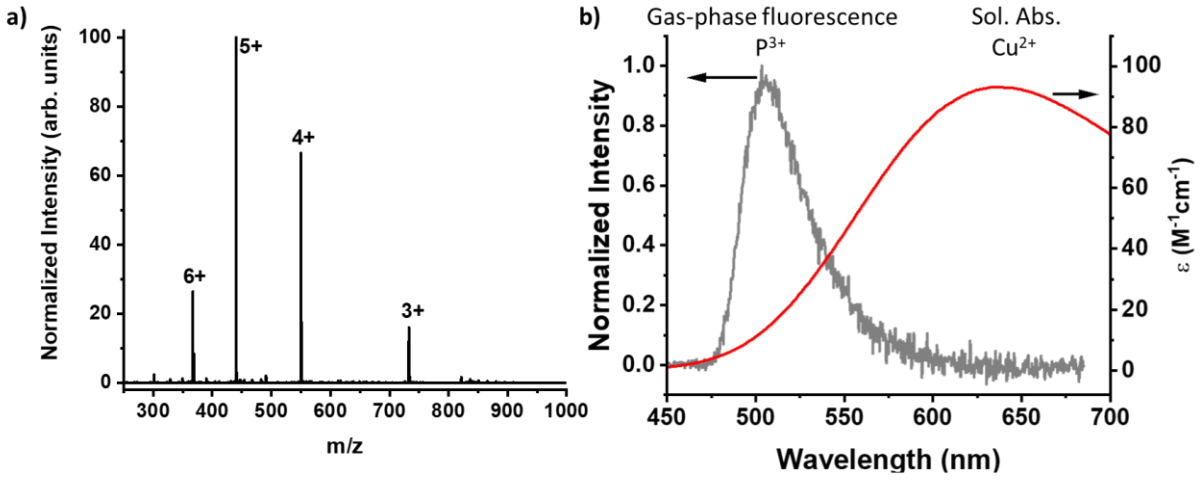

Figure S5: a) Mass spectrum of the peptide labeled with carboxyrhodamine 6g dye showing different charge states of the dye labeled peptide. b) Overlap of donor (carboxyrhodamine 6g) emission conjugated with the peptide in the gas phase (3+ charge state) and the acceptor absorption (Cu^{2+}, complexed with histidine). An overlap between these spectra confirmed the possibility of tmFRET.

Gas-phase fluorescence lifetimes of bare dye labeled peptide in 3+ charge state and its Cu^{2+} complex in 5+ charge state were extracted from respective fluorescence decays and a significant decrease in fluorescence lifetime of the donor can be observed (Figure S6), indicating occurrence of tmFRET.

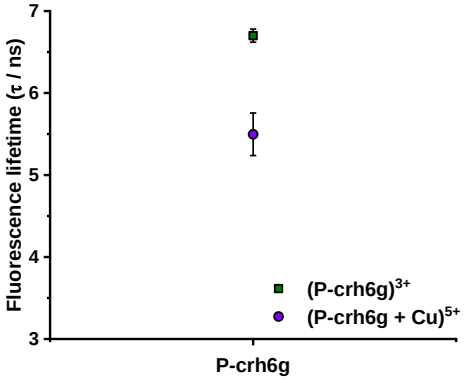

Figure S6: Fluorescence lifetime of dye labeled to the peptide in 3+ charge state with and without bound Cu^{2+}. Clear decrease in fluorescence lifetime in presence of Cu^{2+} indicates the occurrence of tmFRET. P: CAARAHAAAHARAARA.

The control experiments validate that the Cu^{2+} ions bind with high affinity with di-his containing peptides. There is no change in the dye's photophysics upon the binding of the transition metal ion. c) and d) confirm that the decrease in fluorescence lifetime was only in the presence of a tmFRET ion. d) and e) confirm that a decrease in fluorescence lifetime of the donor occurs with other donors and acceptors as well, strengthening the claim that tmFRET takes place in these gaseous peptide complexes.

Other fluorescence quenching mechanisms, like electron transfer and spin-orbit coupling, are also unlikely, as the distance ranges where they operate is less than what has been modeled and measured in the systems studied in this work. Even for smaller donor-acceptor distances (below 10 Å) in similar systems, the energy transfer mechanism has been shown to be FRET and not electron transfer.[1]

The fluorescence lifetime of the 3+ charge state after Cu^{2+} complexation did not show any considerable change with varying donor-acceptor distances. There can be multiple reasons for the absence of a lifetime change in the 3+ charge state. It has been reported that when the dye and the transition metal ion are too close, there is no decrease in fluorescence lifetime in the solution.[3] The dye and Cu^{2+} ion might be closer in the 3+ charge state compared to the 5+ charge state, where peptide ions are expected to have an elongated structure. The difference in orbital overlap, which is not shielded in the gas phase compared to that in solution, might also have played a role.

5. Distance estimation from FRET efficiencies

The FRET efficiencies were calculated from the measured fluorescence lifetimes using equation (1). To estimate the donor-acceptor distance (r_{DA}) using the FRET efficiencies (E), the following equation can be used:

$$r_{DA} = R_{0,\,gas} \times (1/E - 1)^{1/6} \quad \text{(S1)}$$

where $R_{0,\,gas}$ is the Förster distance in the gas phase. The Förster distance is unique for a donor-acceptor pair in a given medium and is defined as a distance between the donor and the acceptor at which the FRET efficiency is 0.5. To get an estimate of r_{DA}, it is critical to have a reasonable estimate of $R_{0,\,gas}$. The following equation is used to calculate R_0:

$$R_0 = 0.02108 \left[\frac{\kappa^2 \Phi_D}{n^4} \times J\right]^{\frac{1}{6}} \quad \text{(S2)}$$

where

R_0 is the Förster distance in nm;

κ^2 is an estimate of relative orientation of the donor and acceptor transition dipole moments. Its value ranges from 0 to 4 and the dynamically averaged value, when both donor and acceptor are supposed to be freely moving about their positions, is 2/3;

Φ_D is the fluorescence quantum yield of the donor in the absence of any acceptor;

J is the spectral overlap between the donor emission and the acceptor absorption with units in the form $mol^{-1}dm^{-3}cm^{-1}nm^4$;

n is the refractive index of the medium.

Directly estimating R_0 in the gas phase is not currently possible, as values for Φ_D and for the absorption of the acceptor in the gas phase are difficult to obtain. However, an estimate of R_0 in the gas phase can be obtained from the corresponding solution-phase value. The methodology to obtain the estimates is discussed in detail in the literature.[4] The solution phase R_0 for rhodamine 110 and Cu^{2+} was calculated using equation S2 and was found to be **18 Å**. A dynamically averaged value of κ^2 was assumed. The quantum yield of the rhodamine 110 dye has been reported to be ~1.[5] J was calculated using the solution-phase fluorescence emission spectrum of peptide labeled with rhodamine 110 and the absorption spectrum of $CuCl_2$ solution in water with 8-fold excess of histidine, and was found to be 2.967×10^{12} $nm^4/(M*cm)$. The refractive index of water was taken to be 1.33.

To estimate R_0 in the gas phase, estimates of parameters in equation S2 were taken based on those in the literature.[4] κ^2 was assumed to be 2/3 in the gas phase as well. Φ_D and *J* were also estimated to remain largely unchanged. The fluorescence spectrum of the dye is found to blue-shifted in the gas phase and the absorbance of Cu^{2+} is also expected to shift as the absorption cross-section is expected to decrease by ~3% following the Spherical Cavity Model.[4,6] Any minor changes in values of Φ_D and *J* are unlikely to have a significant impact on the R_0 estimate because of their inverse sixth power dependence with R_0. The refractive index in vacuum was taken as 1. The change in the refractive index from solution to vacuum has the largest impact on the R_0 value, increasing it by ~21%.[4] Using these approximations, the gas-phase R_0

($R_{0,\,gas}$) was estimated to be **21.8 Å**. Equation S1 was used to obtain an estimate of the distances in different peptides (Table S2).

Table S2: Measured FRET efficiencies in the gas phase with corresponding estimated donor-acceptor separations

Peptide	E	r_{DA} (Å)
C2H3H7	0.7	18.6
C2H6H10	0.4	23.3
C2H10H14	0.3	25.4

6. Binding site of Cu^{2+} in the peptide

The selective binding of Cu^{2+} with peptide ions in the gas phase was confirmed and demonstrated in Figure S1. It has been postulated that in the solution phase, the Cu^{2+} is complexed by both histidines of the histidine pair in the sequence.[1] However, upon transition to the gas phase and a possible loss of helicity, binding with both histidines is no longer guaranteed, as they may be spatially separated. To determine where the Cu^{2+} ion binds, we performed Collision Induced Dissociation (CID) experiments and molecular mechanics calculations.

Insight from Collision Induced Dissociation experiments

The summary of the results from the CID experiments is shown in Figure S7. The CID mass spectra and peak assignments for all three peptide complexes are provided in the "CID results" section on page 10. The mass spectra and peak assignments can also be found in that section. From the fragments identified from the CID experiments, no y ions were found with Cu^{2+} complexed with the histidine farther away from the cysteine. In the case of the C2H6H10 and C2H10H14 sequences, b ions with Cu^{2+} bound to fragments with histidine close to cysteine were identified. For C2H3H7, ions corresponding to fragments with both histidines present are marked, indicating that the Cu^{2+} was bound somewhere between H3 and H7.

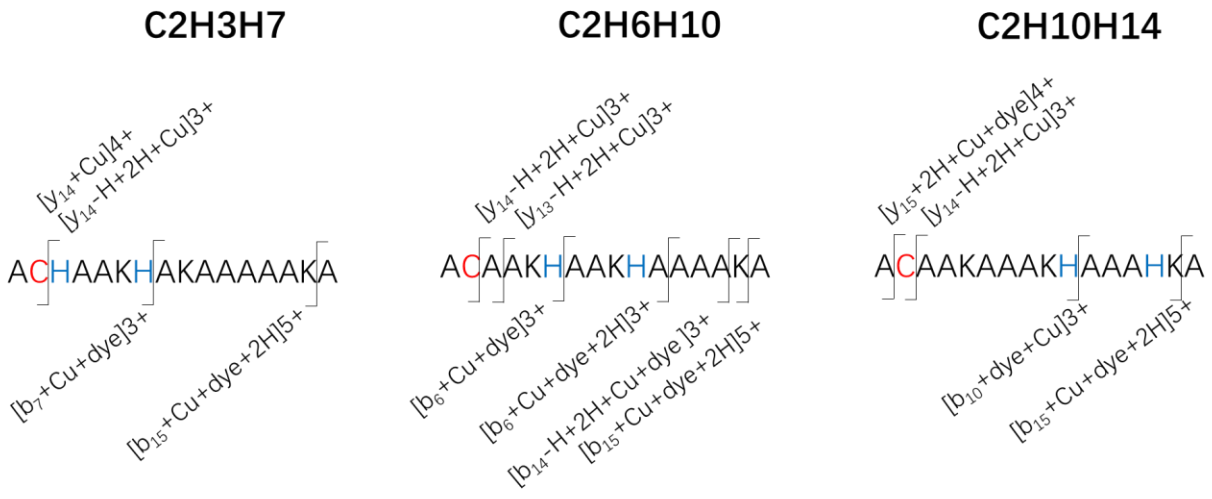

Figure S7: The fragments identified from CID experiments on the 5+ charge states of different peptide ions complexed with Cu^{2+}.

Molecular mechanics calculations indicate the binding site of Cu^{2+}

The structures of the peptides were generated using Chem3D Ultra 19.0.0.22 (PerkinElmer, USA). They were subjected to energy minimization by the MM2 method. The default values of the MM2 force field parameters in the software programs were used for all calculations. In our preliminary MM2 energy minimization, three protons were energetically favored to sit on the amine groups in the first two lysines and the amide group of the amidated c-terminal. Then, the copper ion was added randomly (data not presented) or between two histidines for further MM2 energy minimization. MMFF94 minimization was also employed for verification. MD simulations were not carried out as the overall size of the molecules were too large to attain equilibrium.

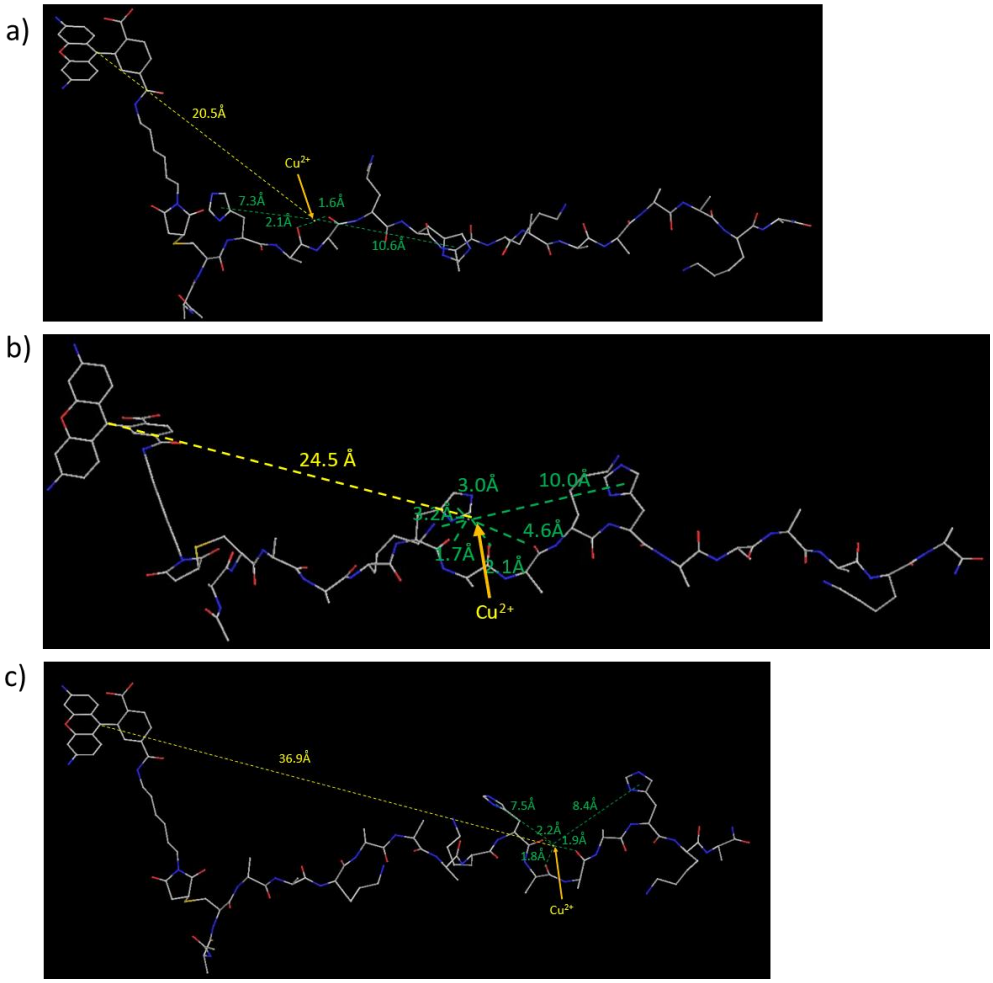

Figure S8: *The energy minimized structures of a) C2H3H7, b) C2H6H10, and c) C2H10H14 showing the binding site of the Cu^{2+} ion and the corresponding distances to nearby atoms.* Minimum separation between the donor and the acceptor is also marked in each figure.

From CID experiments and MM2 optimized structures, a relatively clear picture about the binding site of Cu^{2+} in the gas phase emerges: the Cu^{2+} ion was not found to be complexed with both histidines, as proposed for the solution phase.[1,7] Rather, it was complexed by carbonyl groups near the histidine closer to the cysteine. Molecular dynamics simulations were performed to further understand the structure of complex in the gas phase.

Molecular Dynamics simulations to estimate donor acceptor distances

Molecular dynamics methodology: The initial structures of the peptides were prepared with the AmberTools 20 package, and relaxed using the steepest descent algorithm followed by a short molecular dynamics run (AMBER ff14SB force field). The dye was then introduced using the Avogadro 1.2 molecular editor, and the Cu2+ ion was placed either at one of the two histidine residues, or in between them. From this point onwards, calculations were carried out with the xtb 6.4.0 program, a package for calculations within the Density Functional Tight Binding and related levels of theory. The partially polarizable generalized force field GFN-FF [Spicher, S.; Grimme, S. Angew. Chem. Int. Ed. 2020, 59, 15665–15673] was used to provide an unbiased description of the metal center (the GFN-FF force field is based on an element-specific parameterization, and a set of bond, angle, torsion and charge parameters is generated specifically to suit the provided molecular topology). Initial energy minimization for each model was followed by molecular dynamics run split into two parts. First, an equilibration (thermalization) run of 0.5 ns was carried out, and further 1.5 ns of the simulation was treated as the production run. The time step of 2 fs was used for propagation of equations of motion. The visualization of the results (structures, Figure S9) and calculation of Cu-C(xanthene) radial distribution functions (RDFs) were performed with the VMD 1.9.3 software. The RDF was calculated with 0.1 Å resolution (Figure S10).

Protonation sites: The protonation states were assigned from the pKa analysis, i.e. the three lysine residues were protonated, the zwitterionic ends were retained, and the histidine residues were left at the neutral state to facilitate coordination to the metal.

Metal binding: Addition of a metal center was carried out using, at first, a "free ion" approach and placing it at the histidine N atoms or close to the backbone functions. Energy minimization and short MD runs revealed that the Cu(2+) ions placed along the backbone quickly dissociated from the peptide, and those at the histidine nitrogen atoms were stable. The production runs of the MD assumed, for stability, the fixed bond of His-N-Cu. No assessment of binding energetics was however performed.

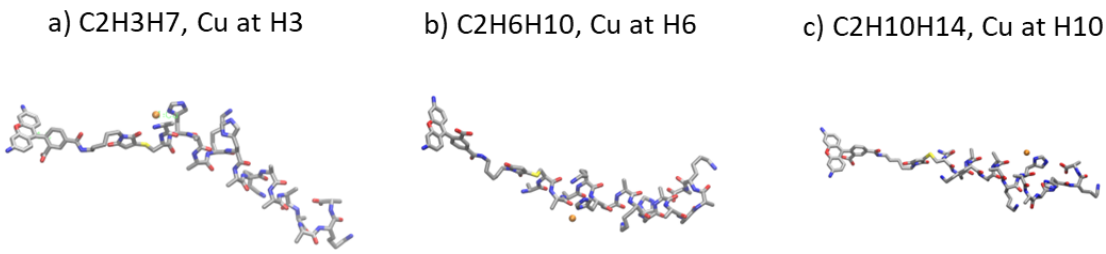

Figure S9: Snapshots form the molecular dynamics simulations showing the structures of the peptide – Cu^{2+} complexes. a) C2H3H7; b) C2HH10; c) C2H10H14.

Distance estimates:

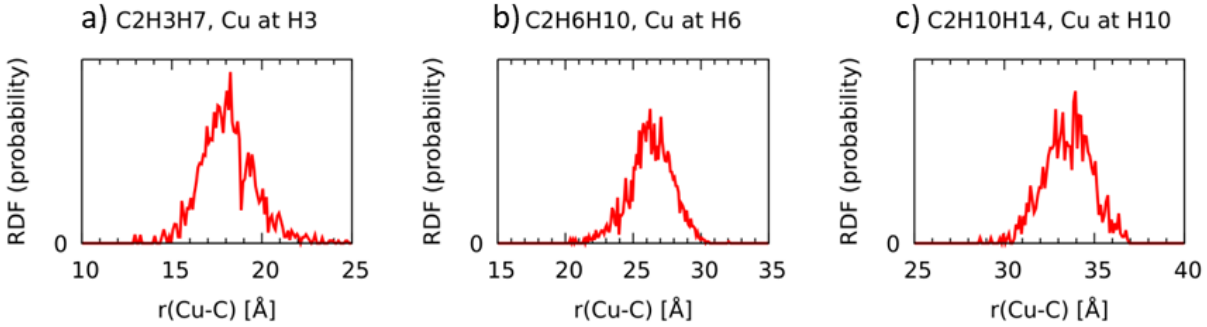

Figure S10: Radial distribution functions (probability densities) for the Cu^{2+} - C (xanthene, central) distances for a) C2H3H7; b) C2H6H10; c) C2H10H14.

The binding site of Cu^{2+} is predicted to be slightly different in case of these MD simulated structures compared to the MM2 energy minimized structures. These may be a result of different nature of force fields used. However, this does not influence the distance prediction much as the metal cations are bound (close) to first histidine and the modeled distances from both methods are within 7 – 12% range of each other.

Comparison of the estimated distances

Estimated distances vs. Modeled distances:

The donor-acceptor distances estimated from tmFRET experiments (Table S2) correlate with the modeled distances obtained from the energy minimized structures and those obtained from MD simulations (Figure S11). A slight underestimation of the distance is expected because of the flexible linker connecting the peptide chain and the donor dye.[1,8]

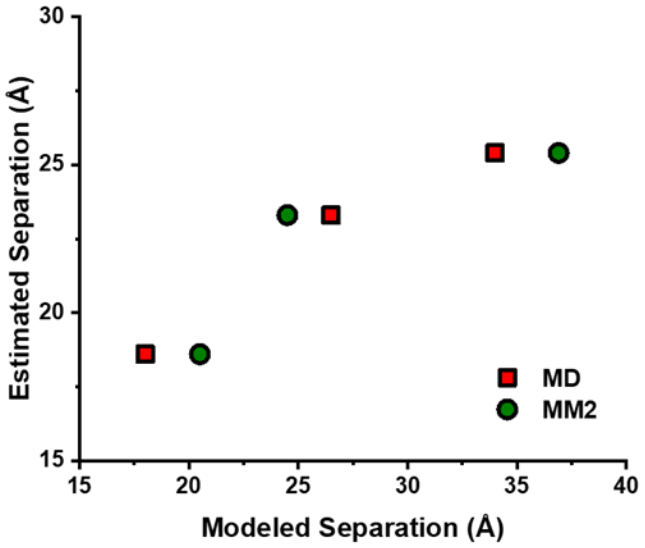

Figure S11: A plot showing the relation between the modeled donor-acceptor distances obtained from the energy-minimized structures and MD simulations vs. the tmFRET estimated donor-acceptor distances.

Inverse sixth power dependence

A comparison of experimentally obtained FRET efficiency values with the modeled values is presented in Figure S12. Experimentally obtained values are close to the modeled FRET efficiencies. However, the observed divergence may be because of a) unavoidable inaccuracies in R_0 estimation,[9,10] and/or b) deviation from the inverse sixth power dependence of FRET efficiency with distances at low donor-acceptor separations.[11,12]

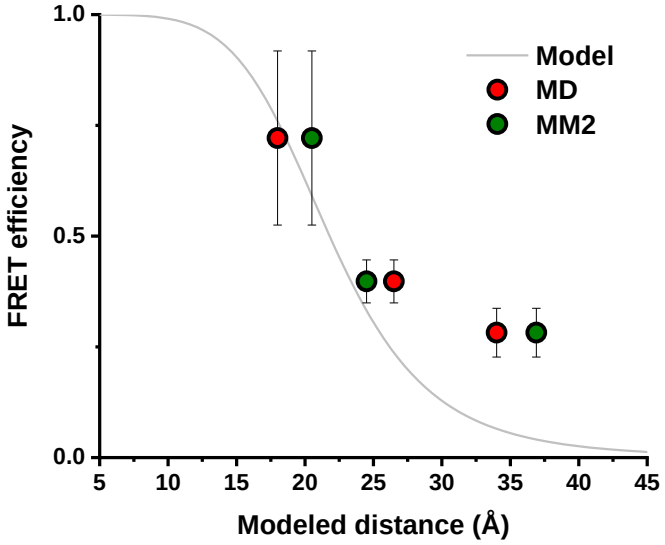

Figure S12: Comparison of experimentally obtained FRET efficiencies (green circles) and the theoretical FRET efficiencies expected for R_0 = 21.8 Å (solid line) with different modeled minimum donor-acceptor separation in peptides.

As mentioned in the main text, the mechanisms of tmFRET need to be understood in greater detail to establish the distance relationship with the FRET efficiency. Even after accounting for changes in fluorophore properties, uncertainties in Cu^{2+} binding site and unavoidable experimental uncertainties, estimated distances from tmFRET measurements seem to correlate with the modeled distances derived using MM2 energy optimization and MD simulation structures (Figure S11). Slight deviation from theoretical FRET efficiency may be due to the uncertainties mentioned above, or because of a different relation of FRET efficiency with donor – acceptor distances in short range in the gas phase.

CID results

CID experiment was conducted at Orbitrap (Q-Exactive Plus Standard, 0726030, Thermofisher USA) with calibration using Pierce Ion Calibration Solution (Thermofisher, USA). Acquired mass spectrum data were extracted to txt file and then charge deconvoluted by using mMass software (Version 5.5.0, www.mmass.org). Default processing parameters for peak picking and charge deconvolution were applied and optimized for accurate assignment of monoisotopic peak. The summary of CID product ions was also prepared for reference.

1. CID mass spectra

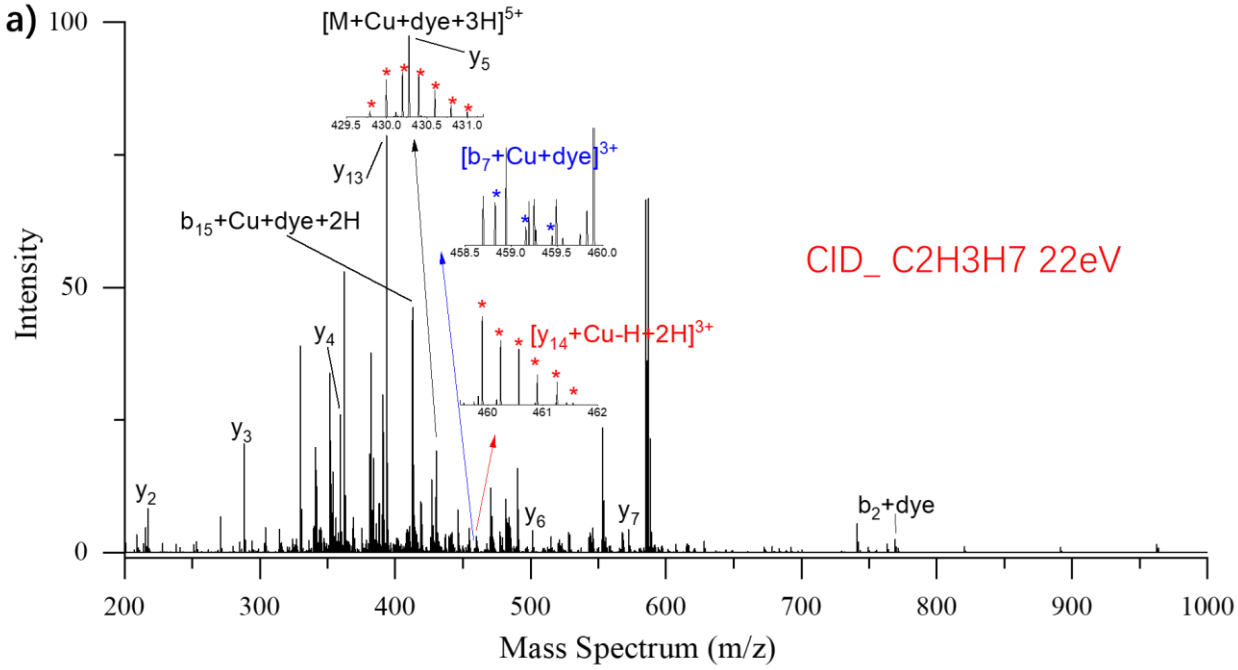

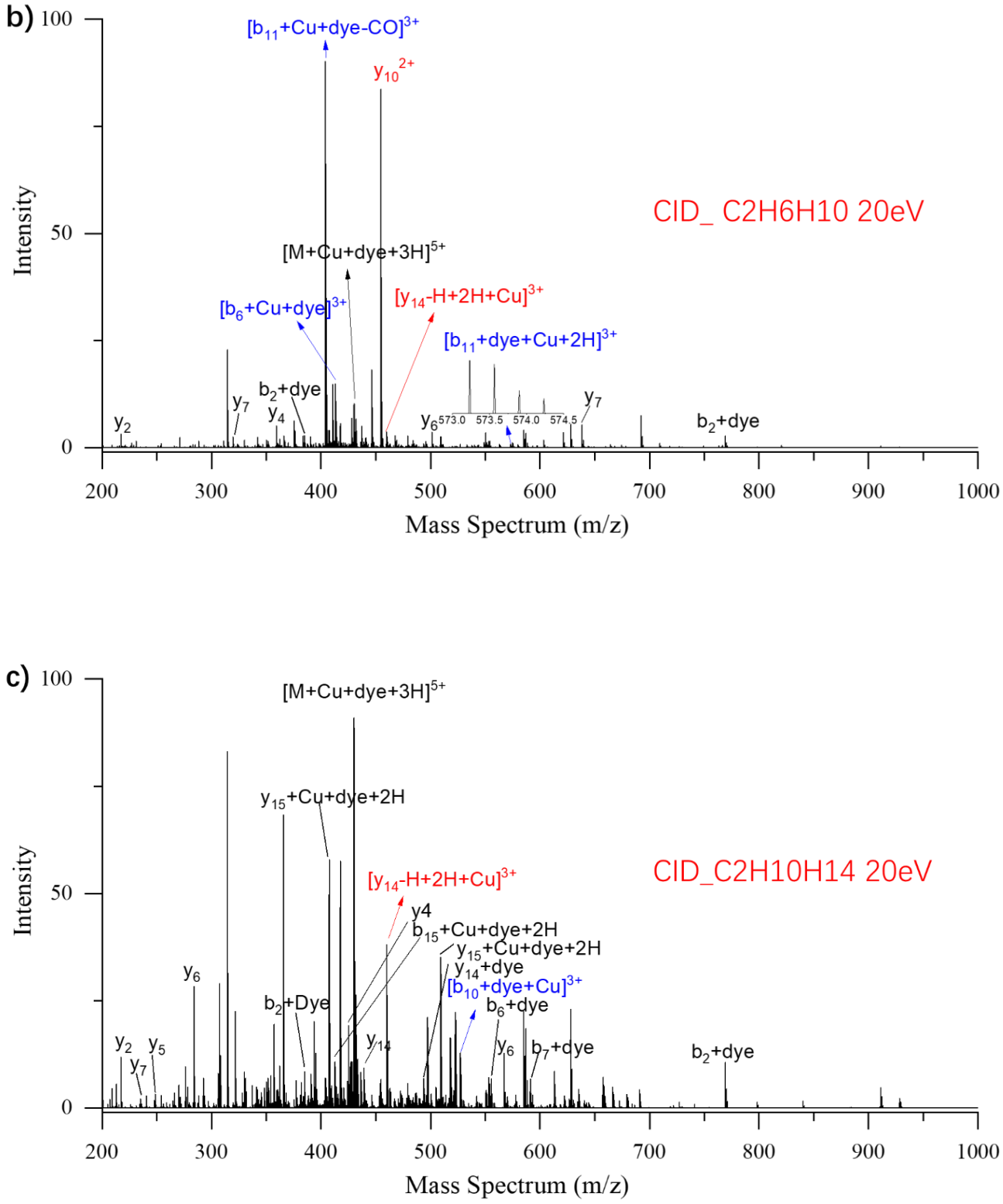

Figure S13: Collision Induced Dissociation of peptide complex ions showing key ion fragments that were identified. a) C2H3H7; b) C2H6H10; and c) C2H10H14.

2. CID ion fragment assignment

Table S3. Summary of CID product ions spectra of $[C2H3H7+Cu]^{5+}$.

Deconvoluted m/z	Assignment	Experimental m/z	Theoretical m/z	Error (ppm)	Int.	r. int.	s/n	z	fwhm	resol.
430.2774	y5	215.6423	215.6423	0.4	9231	6.0	2354.0	2	0.0029	74478
217.1659	y2	217.1659	217.1653	3.0	16195	10.6	4070.7	1	0.0030	72863
501.3143	y6	251.1608	251.1608	0.0	2909	1.9	546.1	2	0.0036	69513
572.3516	y7	286.6794	286.6794	0.3	1292	0.8	185.9	2	0.0044	65278
288.2031	y3	288.2031	288.2025	2.0	39916	26.1	5677.5	1	0.0046	62872
908.5424	y10	303.5190	303.5192	-0.6	3354	2.2	429.3	3	0.0048	62753
1376.6801	y14+Cu	344.9255	344.9267	-3.6	6970	4.6	718.5	4	0.0060	57067
700.4465	y8	350.7269	350.7269	0.2	2652	1.7	266.6	2	0.0061	57341
359.2402	y4	359.2402	359.2396	1.6	50913	33.3	4937.6	1	0.0064	56280
1107.6748	y12	369.8965	369.8965	-0.2	5147	3.4	480.7	3	0.0065	56712
771.4838	y9	386.2455	386.2454	0.4	10465	6.8	953.1	2	0.0070	54897
1178.7114	y13	393.5753	393.5756	-0.6	152924	100.0	13775.8	3	0.0073	54057
2058.8820	b15+Cu+dye+2H	412.5822	412.5850	-6.7	79367	51.9	6952.6	5	0.0078	52991
430.2774	y5	430.2774	430.2767	1.6	38149	24.9	3372.9	1	0.0084	51346
906.3236	b3+dye	453.6655	453.6659	-0.9	2365	1.5	215.8	2	0.0086	52473

908.5427	y10	454.7750	454.7749	0.4	9106	6.0	832.4	2	0.0090	50594
1374.4668	b7+Cu+dye	458.8271	458.8270	0.2	718	0.5	66.0	3	0.0096	47960
1377.6921	y14+Cu-H+2H	459.9022	459.9023	-0.1	5934	3.9	546.3	3	0.0092	49903
977.3608	b4+dye	489.1840	489.1844	-0.7	2108	1.4	212.3	2	0.0099	49228
501.3144	y6	501.3144	501.3138	1.1	8118	5.3	856.8	1	0.0104	48381
572.3517	y7	572.3517	572.3509	1.5	8613	5.6	1328.4	1	0.0121	47118
624.2932	b6	624.2932	624.2928	0.7	145	0.1	31.1	1	0.0139	44872
700.4470	y8	700.4470	700.4459	1.6	966	0.6	300.6	1	0.0176	39701
769.2650	b2+dye	769.2650	769.2650	0.0	4843	3.2	1961.3	1	0.0196	39314
771.4837	y9	771.4837	771.4830	0.9	1569	1.0	641.3	1	0.0205	37691

Table S4. Summary of CID product ions spectra of $[C2H6H10+Cu]^{5+}$.

Deconvoluted m/z	Assignment	Experimental m/z	Theoretical m/z	Error (ppm)	Int.	r. int.	s/n	z	fwhm	resol.
430.2774	y5	215.6423	215.6423	0.4	1150	0.3	230.9	2	0.0029	73346
217.1660	y2	217.1660	217.1653	3.2	14195	3.5	2805.7	1	0.0030	71822
501.3143	y6	251.1608	251.1608	0.1	1774	0.4	252.0	2	0.0036	68892
288.2031	y3	288.2031	288.2025	1.9	6483	1.6	672.0	1	0.0046	62908
908.5425	y10	303.5190	303.5192	-0.4	2336	0.6	214.8	3	0.0048	62778
638.3736	y7	319.6904	319.6903	0.6	11005	2.7	904.5	2	0.0054	58895
359.2403	y4	359.2403	359.2396	1.8	22782	5.7	1494.4	1	0.0065	55570
766.4684	y8	383.7379	383.7378	0.3	11793	2.9	705.5	2	0.0070	54585
769.2654	b2+dye	385.1364	385.1364	-0.1	12142	3.0	723.3	2	0.0071	54462
1173.6983	y12	391.9043	391.9038	1.3	262	0.1	15.3	3	0.0071	55070
1176.4933	b6+dye	392.8360	392.8362	-0.7	2626	0.7	152.9	3	0.0071	54945
1209.4131	b6+Cu+dye-CO	403.8092	403.8091	0.4	400659	100.0	22591.2	3	0.0075	53575
2058.8819	b15+Cu+dye+2H	412.5822	412.5850	-6.7	6733	1.7	370.3	5	0.0077	53663
1237.4074	b6+Cu+dye	413.1407	413.1407	-0.2	65967	16.5	3622.8	3	0.0080	51511
837.5054	y9	419.2564	419.2563	0.1	4793	1.2	259.7	2	0.0081	51988
840.3024	b3+dye	420.6548	420.6550	-0.3	4891	1.2	264.8	2	0.0079	53241

430.2775	y5	430.2775	430.2767	1.8	28586	7.1	1538.1	1	0.0085	50822
1725.7955	b12+dye	432.2043	432.2047	-0.8	8397	2.1	451.3	4	0.0081	53099
1306.6544	y13-H+2H+Cu	436.2230	436.2232	-0.5	5498	1.4	294.8	3	0.0087	50381
1315.6751	b14	439.2299	439.2283	3.6	2520	0.6	134.8	3	0.0078	56275
1315.7711	y14	439.2619	439.2619	0.1	5667	1.4	303.2	3	0.0086	50941
1318.5689	b8+dye	440.1945	440.1943	0.5	2253	0.6	120.5	3	0.0090	49160
908.5427	y10	454.7750	454.7749	0.3	369617	92.3	19590.8	2	0.0092	49681
911.3392	b4+dye	456.1733	456.1735	-0.5	1485	0.4	78.6	2	0.0091	49930
1377.6922	y14-H+2H+Cu	459.9023	459.9023	-0.1	16048	4.0	848.0	3	0.0093	49342
487.2371	b5	487.2371	487.2339	6.5	2836	0.7	152.5	1	0.0099	49131
1970.9808	y15+dye	493.5007	493.5007	-0.1	3937	1.0	213.2	4	0.0098	50122
501.3144	y6	501.3144	501.3138	1.3	15814	3.9	864.0	1	0.0104	48164
1045.6020	y11	523.3047	523.3043	0.7	327	0.1	18.4	2	0.0112	46614
1583.7256	b10+dye	528.5801	528.5789	2.1	168	0.0	9.6	3	0.0120	43998
1654.7584	b11+dye	552.2577	552.2580	-0.6	794	0.2	47.5	3	0.0120	46135
1717.6826	b11+dye+Cu+2H	573.2324	573.2343	-3.3	3262	0.8	204.4	3	0.0122	47047
1176.4930	b6+dye	588.7502	588.7505	-0.5	1754	0.4	113.9	2	0.0126	46619
1867.8684	b14+dye	623.2943	623.2951	-1.2	550	0.1	38.8	3	0.0150	41455
1247.5306	b7+dye	624.2689	624.2690	-0.1	571	0.1	40.4	2	0.0148	42066

638.3734	y7	638.3734	638.3727	1.1	23464	5.9	1719.0	1	0.0149	42956
1929.7923	b14-H+2H+Cu+dye	643.9356	643.9355	0.2	1071	0.3	79.6	3	0.0157	40982
1318.5674	b8+dye	659.7873	659.7876	-0.3	1012	0.3	78.3	2	0.0160	41272
766.4680	y8	766.4680	766.4677	0.4	2219	0.6	263.9	1	0.0185	41380
769.2650	b2+dye	769.2650	769.2650	0.0	12036	3.0	1454.3	1	0.0196	39149
840.2995	b3+dye	840.2995	840.3021	-3.1	224	0.1	45.0	1	0.0228	36796
911.3379	b4+dye	911.3379	911.3392	-1.5	1820	0.5	724.3	1	0.0254	35944
1039.4330	b5+dye	1039.4330	1039.4342	-1.1	134	0.0	283.1	1	0.0315	32959

Table S5. Summary of CID product ions spectra of $[C2H10H14+Cu]^{5+}$.

Deconvoluted m/z	Assignment	Experimental m/z	Theoretical m/z	Error (ppm)	Int.	r. int.	s/n	z	fwhm	resol.
217.1663	y2	217.1660	217.1653	3.2	17652.6	13.3	1624.7	1	0.0030	71978
704.3963	y7	235.4700	235.4700333	-0.3	2380.7	1.8	189.3	3	0.0032	73324
496.2989	y5	248.6532	248.65315	0.2	4707.3	3.5	340.7	2	0.0036	68160
567.3371	y6	284.1718	284.1717	0.4	41668.9	31.4	2345.2	2	0.0046	62092
1315.7717	y14	329.6982	329.6984	-0.4	1254.1	0.9	52.7	4	0.0055	59799
1376.6817	y14+Cu	344.9265	344.926725	-0.6	1104.8	0.8	42.8	4	0.0062	55763
704.3949	y7	352.7014	352.70115	0.6	5892.1	4.4	219.3	2	0.0063	56371
354.2247	y3	354.2249	354.2242	2.1	11058.6	8.3	408.5	1	0.0062	56946
769.2659	b2+dye	385.1363	385.1364	-0.1	12377.9	9.3	404.5	2	0.0070	55056
2033.9058	y15+Cu+dye+2H	407.5869	407.5879	-2.6	86010.9	64.8	2620.7	5	0.0077	52784
2058.8823	b15+Cu+dye+2H	412.5822	412.585	-6.8	14399.5	10.8	432.2	5	0.0078	53221
1244.7347	y13	415.5816	415.5828333	-2.9	4698.7	3.5	139.8	3	0.0085	48658
840.302594	b3+dye	420.6549	420.65495	-0.2	6971.4	5.3	205.5	2	0.0079	53485
425.2624	y4	425.2621	425.2614	1.8	28262.5	21.3	829.0	1	0.0081	52243
1315.772	y14	439.2618	439.2618667	-0.1	13605.3	10.2	393.2	3	0.0087	50577
903.5287	y9	452.2676	452.2672	0.9	439.9	0.3	12.5	2	0.0087	52172

1377.6935	y14-H+2H+Cu	459.9025	459.9023	0.5	56173.7	42.3	1589.1	3	0.0092	49972
1970.9801	y14+dye	493.5007	493.5007	0.0	8933.8	6.7	256.4	4	0.0101	48646
496.2989	y5	496.2993	496.2985	1.5	4401.3	3.3	126.6	1	0.0102	48716
1517.702	b10+dye	506.5716	506.5716667	-0.1	2117.7	1.6	61.5	3	0.0099	51044
2033.9057	y15+Cu+dye+2H	509.2319	509.233	-2.1	52526.3	39.6	1528.5	4	0.0106	47865
1039.4343	b5+dye	520.2193	520.221	-3.2	1356.7	1.0	40.0	2	0.0123	42464
1045.6003	y11	523.3039	523.3043	-0.8	1619.2	1.2	48.1	2	0.0104	50523
1578.6125	b10+dye+Cu	526.8761	526.8761667	-0.1	16582.2	12.5	496.8	3	0.0114	46420
1588.7342	b11+dye	530.2508	530.2506667	0.3	2533.2	1.9	76.5	3	0.0115	46243
1110.4699	b6+dye	555.7394	555.73955	-0.3	9946.3	7.5	319.9	2	0.0125	44638
567.3358	y6	567.3364	567.3356	1.5	18681.3	14.1	619.0	1	0.0127	44604
1181.5081	b7+dye	591.2572	591.2581	-1.6	9838.6	7.4	354.0	2	0.0135	43665
1252.5495	b8+dye	626.7764	626.77665	-0.3	3085.1	2.3	127.2	2	0.0147	42612
1380.6429	b9+dye	690.8240	690.8242	-0.2	6266.4	4.7	344.8	2	0.0169	40911
704.3937	y7	704.3944	704.3945	-0.1	120.3	0.1	7.1	1	0.0172	40978
769.2659	b2+dye	769.2650	769.265	0.0	15505.0	11.7	1300.0	1	0.0196	39220
840.2987	b3+dye	840.3019	840.3021	-0.2	2350.0	1.8	304.4	1	0.0216	38894
911.3424	b4+dye	911.3392	911.3392	0.0	7090.9	5.3	1553.0	1	0.0257	35474

7. References

(1) Taraska, J. W.; Puljung, M. C.; Zagotta, W. N. Short-Distance Probes for Protein Backbone Structure Based on Energy Transfer between Bimane and Transition Metal Ions. *Proc. Natl. Acad. Sci. U. S. A.* **2009**, *106* (38), 16227–16232.

(2) Tiwari, P.; Metternich, J. B.; Czar, M. F.; Zenobi, R. Breaking the Brightness Barrier: Design and Characterization of a Selected-Ion Fluorescence Measurement Setup with High Optical Detection Efficiency. *J. Am. Soc. Mass Spectrom.* **2021**, *32*, 187–197.

(3) Posokhov, Y. O.; Kyrychenko, A.; Ladokhin, A. S. Steady-State and Time-Resolved Fluorescence Quenching with Transition Metal Ions as Short-Distance Probes for Protein Conformation. *Anal. Biochem.* **2010**, *407* (2), 284–286.

(4) Czar, M. F.; Zosel, F.; König, I.; Nettels, D.; Wunderlich, B.; Schuler, B.; Zarrine-Afsar, A.; Jockusch, R. A. Gas-Phase FRET Efficiency Measurements to Probe the Conformation of Mass-Selected Proteins. *Anal. Chem.* **2015**, *87* (15), 7559–7565.

(5) Kubin, R. F.; Fletcher, A. N. Fluorescence Quantum Yields of Some Rhodamine Dyes. *J. Lumin.* **1982**, *27* (4), 455–462.

(6) Toptygin, D. Effects of the Solvent Refractive Index and Its Dispersion on the Radiative Decay Rate and Extinction Coefficient of a Fluorescent Solute. *J. Fluoresc.* **2003**, *13* (3), 201–219.

(7) Yu, X.; Wu, X.; Bermejo, G. A.; Brooks, B. R.; Taraska, J. W. Accurate High-Throughput Structure Mapping and Prediction with Transition Metal Ion FRET. *Structure* **2013**, *21* (1), 9–19.

(8) Wiczk, W.; Eis, P. S.; Fishman, M. N.; Johnson, M. L.; Lakowicz, J. R. Distance Distributions Recovered from Steady-State Fluorescence Measurements on Thirteen Donor-Acceptor Pairs with Different Förster Distances. *J. Fluoresc.* **1991**, *1* (4), 273–286.

(9) Czar, M. F.; Zosel, F.; Koenig, I.; Nettels, D.; Wunderlich, B.; Schuler, B.; Zarrine-Afsar, A.; Jockusch, R. A. Gas-Phase FRET Efficiency Measurements to Probe the Conformation of Mass-Selected Proteins. *Anal. Chem.* **2015**, *87* (15), 7559–7565.

(10) Talbot, F. O.; Rullo, A.; Yao, H.; Jockusch, R. A. Fluorescence Resonance Energy Transfer in Gaseous, Mass-Selected Polyproline Peptides. *J. Am. Chem. Soc.* **2010**, *132* (45), 16156–16164.

(11) Dominik Spiegel, J.; Fulle, S.; Kleinschmidt, M.; Gohlke, H.; Marian, C. M. Failure of the IDA in FRET Systems at Close Inter-Dye Distances Is Moderated by Frequent Low K2 Values. *J. Phys. Chem. B* **2016**, *120* (34), 8845–8862.

(12) Schuler, B.; Lipman, E. A.; Steinbach, P. J.; Kumkell, M.; Eaton, W. A. Polyproline and the "Spectroscopic Ruler" Revisited with Single-Molecule Flourescence. *Proc. Natl. Acad. Sci. U. S. A.* **2005**, *102* (8), 2754–2759.